Equilibrium Spectra of Wind Waves

MICHAEL L. BANNER

School of Mathematics, University of New South Wales, Kensington, N.S.W., Australia

(Manuscript received 25 July 1989, in final form 14 December 1989)

ABSTRACT

Equilibrium spectral behavior for ocean gravity wind waves has been investigated actively over the past three decades, yet fundamental problems remain in reconciling theory with observations. Predicted equilibrium spectral forms from physical models proposed recently by Kitaigorodskii and by Phillips are examined in the light of wavenumber and frequency spectra reported by several investigators. While frequency domain observations appear to support the model predictions, observed wavenumber spectra are found to differ both in the spectral dependence on wavenumber and on the wind speed.

Based on observed wavenumber and frequency spectra for fetch-limited conditions, a model is proposed for the form of the directional wavenumber spectrum slice in the dominant wave direction. Reduced wavenumber and frequency spectra are calculated from this model, assuming an empirical spectral directional spreading function and the linear gravity wave dispersion relation. These calculations reveal the underlying influences which shape these reduced spectra. In the energy containing subrange, just above the spectral peak, the dominant influence shaping these spectra is the variation of the directional spreading function with distance from the spectral peak. For frequency spectra, at higher frequencies, the model calculations predict that the range of observed frequency spectral dependences is due primarily to the Doppler shifting from advection of the shorter waves by the orbital motion of the dominant waves, with possible additional influences of wind drift and ambient currents.

Combining these results, composite calculated frequency spectra and one-dimensional wavenumber spectra show close correspondence with measured field spectra. In addition to clarifying the key processes that shape different regimes in the frequency spectrum, a refinement of the bounds of the gravity equilibrium subrange is proposed.

1. Introduction

Ocean wind waves possess a random character, and wave spectra are used to represent mean distributions of wave energy with respect to both spatial and temporal scales of variability. Following Phillips (1977 §4.1) the wave spectrum for a homogeneous, stationary wave field is defined as

$$X(\mathbf{k}, \omega) = (2\pi)^{-3} \int\int_{-\infty}^{\infty} \rho(\mathbf{r}, t) \times \exp[-i(\mathbf{k}\cdot\mathbf{r} - \omega t)]d\mathbf{r}dt \quad (1.1)$$

where $\rho(\mathbf{r}, t) = \overline{\xi(\mathbf{x}, t_0)\xi(\mathbf{x}+\mathbf{r}, t_0+t)}$ is the covariance of the surface displacement $\xi(\mathbf{x}, t)$, $\mathbf{r}$ is the spatial separation vector, t is the time separation, $\mathbf{k}$ $[=(k_1, k_2) = (k, \theta)]$ is the wavenumber vector and ω is the frequency. Here $X(\mathbf{k}, \omega)$ has the property that

$$\int\int_{-\infty}^{\infty} X(\mathbf{k}, \omega)d\mathbf{k}d\omega = \overline{\xi^2},$$

the mean squared waveheight and represents the mean distribution of wave energy with wavenumber magnitude $k = |\mathbf{k}|$ and frequency ω propagating in the direction θ. Various reduced spectra defined below are of theoretical or observational importance, and are referred to frequently in this paper.

(i) the directional wavenumber spectrum

$$\Phi(\mathbf{k}) = 2\int_0^{\infty} X(\mathbf{k}, \omega)d\omega, \quad (1.2)$$

representing the actual wavenumber directional distribution of wave energy propagation.

(ii) wavenumber spectrum

$$\Phi_s(\mathbf{k}) = \int_{-\infty}^{\infty} X(\mathbf{k}, \omega)d\omega, \quad (1.3)$$

representing the folded wavenumber distribution: we note that $\Phi_s(\mathbf{k}) = 0.5[\Phi(\mathbf{k}) + \Phi(-\mathbf{k})]$. The $\Phi_s(\mathbf{k})$ arises from frozen spatial image analysis and does not contain

Corresponding author address: Dr. Michael L. Banner, School of Mathematics, University of New South Wales, P.O. Box 1, Kensington, New South Wales, Australia 2033.

actual wave propagation information, partitioning the wave energy equally to components 180° apart.

(iii) one-dimensional (transverse) spectra

$$\phi(k_1) = \int_{-\infty}^{\infty} \Phi(k_1, k_2)dk_2 \quad \text{and}$$

$$\phi(k_2) = \int_{-\infty}^{\infty} \Phi(k_1, k_2)dk_1 \qquad (1.4)$$

(iv) omnidirectional wavenumber spectrum

$$\bar{\phi}(k) = \int_{-\pi}^{\pi} k\Phi(k, \theta)d\theta \qquad (1.5)$$

representing the waveheight spectral density for wavenumber magnitude k for all directions.

(v) directionally-averaged wavenumber spectrum

$$f(k) = \int_{-\pi}^{\pi} \Phi(k, \theta)d\theta \qquad (1.6)$$

(vi) directional frequency spectrum

$$G(\omega, \theta) = 2\int_{0}^{\infty} X(\mathbf{k}, \omega)kdk \qquad (1.7)$$

(vii) frequency spectrum

$$F(\omega) = \int_{-\pi}^{\pi} G(\omega, \theta)d\theta. \qquad (1.8)$$

The evolution of the directional wavenumber spectrum $\Phi(\mathbf{k}{:}\mathbf{x}, t)$ has been described by Hasselmann (1962, 1963a,b), based on the radiative transfer equation

$$D\Phi/Dt = \partial\Phi/\partial t + \mathbf{c}_g \cdot \nabla\Phi = S_{in} + S_{nl} + S_{\text{diss}}. \qquad (1.9)$$

Here $S_{in}(\mathbf{k})$, $S_{nl}(\mathbf{k})$ and $S_{\text{diss}}(\mathbf{k})$ are the source terms representing the spectral distributions of wind input, nonlinear interactions with other wave components and dissipation, through wave breaking and turbulence. If, for certain subranges of $\mathbf{k}$,

$$D\Phi(\mathbf{k}{:}\mathbf{x}, t)/Dt = \partial\Phi/\partial t + \mathbf{c}_g \cdot \nabla\Phi = 0 \qquad (1.10)$$

then this subrange is in statistical equilibrium and the source terms are in balance. Phillips (1985) presents an authoritative and comprehensive account of equilibrium spectral subranges for gravity wind waves, and provides a more detailed discussion of the concept of spectral statistical equilibrium.

Particular models for the balancing source terms lead to different equilibrium spectral subrange forms. Phillips (1958) pioneering work on the equilibrium spectral form observed for the rear face of the waveheight frequency spectrum at frequencies above the spectral peak, proposed an equilibrium spectral form determined primarily by dissipation through wave breaking, which imposed a fixed upper limit on the spectral level independent of the wind strength. Nonlinear wave–wave interactions were not considered in this model. Dimensional analysis of the proposed physical model predicted the following forms for the gravity wind-wave equilibrium spectral ranges in the frequency and wavenumber domains:

$$F(\omega) = \alpha g^2\omega^{-5}, \quad f(k) = Bk^{-4} \qquad (1.11)$$

where g is the gravitational acceleration and α, B are equilibrium range constants.

Hasselmann (1962, 1963a,b) presented the theoretical underpinnings of the role of weakly nonlinear wave–wave interactions in the spectral evolution of homogeneous random ocean wave fields with approximately Gaussian statistics, expressed by S_{nl} in the evolution equation (1.9). The nonlinear spectral interactions act in conjunction with the wind input and wave dissipation in determining the wave spectrum, implying that a proper understanding and description of all of these source terms may be needed to properly model equilibrium behavior.

a. Observational background

Earlier observational studies, mostly of the frequency spectrum, seemed to offer support for the model (1.11) proposed by Phillips (1958). More recent observational studies (e.g., Toba 1973; Kawai et al. 1977; Kahma 1981; Forristall 1981; Battjes et al. 1987) have shown an increasing body of support for an equilibrium frequency spectrum of the form

$$F(\omega) = \beta g u_* \omega^{-4} \qquad (1.12)$$

for frequencies in the range $1.5 < \omega/\omega_p < \omega_u$, where ω_p is the spectral peak frequency and ω_u is a nondimensional upper frequency bound. Here u_* is the wind friction velocity, which is related to a reference windspeed by a drag coefficient (e.g., see Wu 1980). Phillips (1985, Table 1) and Battjes et al. (1987) reviewed the notable observed variability in the (Toba) constant of proportionality β, noting the absence of any clear dependence on nondimensional fetch, significant slope or nondimensional dominant wave period. The authoritative study by Donelan et al. (1985, henceforth referred to as DHH) has provided the most detailed study of fetch-limited wind wave growth to date. They proposed a relationship for the frequency spectrum just above the spectral peak of the form

$$F(\omega) = 0.006g^2(U_c/c_p)^{0.55}(\omega/\omega_p)\omega^{-5} \qquad (1.13)$$

i.e., an intrinsic dependence on $(U_c/c_p)^{0.55}$ and (ω/ω_p), which represents a refinement over the previous form (1.12). Here U_c is the effective windspeed in the dominant wave direction and c_p is the phase speed of the spectral peak waves.

Amid the increasing support for ω^{-4} dependence, anomalous dependences have also been documented. Forristall (1981) reported hurricane wave frequency spectra which behaved as ω^{-4} just above the spectral peak but transitioned to close to ω^{-5} at higher fre-

quencies. Very recently, for the energy-containing subrange under fetch-limited conditions on Lake Michigan (Liu 1989) reported ω^{-4} dependence for growing windseas while ω^{-3} was found for fully developed spectra.

At frequencies well above the spectral peak, the observed spectral frequency dependence on windspeed is even more variable, depending on the distance from the spectral peak, the wave age and possibly the fetch or duration. For example, Mitsuyasu (1977) reported ω^{-5} for $0.6 < \omega < 4$ Hz, and ω^{-4} for $4 < \omega < 15$ Hz for short fetch and $U_{10.5} = 8$ m s^{-1}; Stolte (1984) found similar trends for the high frequencies, with exponents of $\omega^{-4.2}$ for $U_{19.5} = 3.3$ m s^{-1}, $\omega^{-3.9}$ for $U_{19.5} = 8.9$ m s^{-1}, $\omega^{-3.5}$ for $U_{19.5} = 14.6$ m s^{-1} and $\omega^{-3.3}$ for $U_{19.5} = 19.0$ m s^{-1}. However, these findings are hardly surprising in view of Doppler shifting effects for these components, as analyzed by Kitaigorodskii et al. (1975) and in Banner et al. (1989).

It is well known that the wave field is directional, yet frequency spectra obscure the directionality. This limitation has been addressed by time domain methods based on the wave slope, such as the pitch and roll buoy (e.g., Longuet-Higgins et al. 1963; Mitsuyasu et al. 1975, 1983; Hasselmann et al. 1980). These have provided information on directional spreading characteristics in the frequency domain, but are limited by relatively poor angular resolution.

Owing to increased observational and analysis complexity, fewer spatial domain measurements have been reported, based on arrays of height gauges (e.g., see DHH for a summary) and stereophotogrammetric analysis (e.g., Cote et al. 1962; Holthuijsen 1983; Banner et al. 1989). Remote sensing methods based on radar altimetry (Barnett and Wilkerson 1967), laser altimetry (Schule et al. 1971) and off-nadir radar reflectivity (Walsh et al. 1985; Jackson et al. 1985a,b) have also been used. Also, purely spatial domain observations yield wavenumber spectra $\Phi_s(k, \theta)$ that do not provide information on the actual direction of wave energy propagation, for which a further assumption is needed, to be addressed subsequently. Donelan et al. used an array method to determine wavenumber–frequency spectra from which $\Phi(k, \theta)$ was directly determined near the spectral peak with increased angular resolution. We draw heavily on their results in this study.

b. *Equilibrium range modeling*

Alternative equilibrium range models were proposed recently by Kitaigorodskii (1983) and by Phillips (1985), based on significantly different underlying physical processes. Phillips model predicted an equilibrium wavenumber spectrum of the form

$$\Phi_s(k) \sim u_* g^{-1/2} k^{-7/2} g(\theta), \qquad (1.14)$$

where $g(\theta)$ represents a directional spreading function. The one-dimensional wavenumber and frequency spectral forms corresponding to (1.14) were given as

$$\phi(k_i) \sim u_* g^{-1/2} k_i^{-5/2} \quad \text{for} \quad i = 1, 2 \qquad (1.15)$$

$$F(\omega) \sim u_* g \omega^{-4}. \qquad (1.16)$$

According to Phillips, the equilibrium spectral range covered gravity wave components with wavelengths much shorter than those of the spectral peak. Kitaigorodskii's model predicted (1.14)–(1.16) for $\omega < \omega_g$ and (1.11) for $\omega > \omega_g$, where $\omega_g \sim 4g/U$ is an empirical transition frequency. While recognizing the directionality of the wave field, these authors did not pursue the implications of the directional spreading function dependence on wave age c_p/U or on k/k_p, where k_p is the spectral peak wavenumber. The potential importance of these effects in shaping $F(\omega)$ was noted by DHH. As a basic component of a detailed model for radar backscatter from the sea surface, Donelan and Pierson (1987) proposed a composite wavenumber spectral form for fully developed sea states. This was based on the directional frequency spectral model proposed by DHH near the spectral peak, linked to a higher wavenumber form based on a postulated local equilibrium between wind input and dissipation.

Using (2.4) below, the form of the wavenumber spectrum just above the spectral peak, consistent with the proposed DHH frequency and directional frequency spectral forms [their equations (9.1)–(9.6)] is easily found to be

$$\Phi(k, \theta) = 8.6 \times 10^{-5} (U/c_p)^{0.55} (k_p/k)^{0.15} k^{-4} D(\theta; k/k_p) \qquad (1.17)$$

where D is the directional spreading function proposed by DHH, which is discussed in detail in section 2. However, it is seen that the elegant spectral dependence on (ω/ω_p) in the frequency spectrum (1.13) does not carry over to the wavenumber domain. A slightly modified form determined independently from other wavenumber observations, together with the approximate windspeed dependence found by DHH, is the basis of the wavenumber spectral model adopted here (in §2a), but these differences have little impact on the major results found here.

Despite the apparent support provided for (1.16) in the frequency domain, further confirmation via wavenumber domain measurements is needed to assess independently whether these models are correct (Phillips (1985, p519). A recent study of short ocean gravity waves (Banner et al. 1989) reported wavenumber spectra for 0.2 to 1.6 m wavelengths for a range of sea states and windspeeds. These results are consistent with the one-dimensional wavenumber spectral dependence of k^{-3} found by Schule et al. (1971), and showed a lack of sensitivity to both wind strength and wind direction. These components had a broad directional distribution [within the 180° ambiguity limitation of

$\Phi_s(\mathbf{k})$] and tended to follow a wavenumber spectral dependence of k^{-4}. Thus, the observational results for this short gravity-wave spectral range do not appear to support the equilibrium spectral form (1.15). Despite a possible difference in spectral range of applicability, these differences motivated an amalgamation of this high wavenumber data with the wavenumber data of other studies at lower wavenumbers: the SWOP project (Cote et al. 1962; Schule et al. 1971; Barnett and Wilkerson 1967; Holthuijsen 1983; Jackson et al. 1985a,b) and provide an empirical basis for analyzing some of the problems which challenge existing physical models. In particular, how does one reconcile the observed $\phi(k_i)$ dependence on k_i and its apparent lack of sensitivity to the windspeed at higher wavenumbers with the frequency spectrum observations (and predictions), where a linear or near-linear dependence on u_* has been routinely reported just above the spectral peak, and with other dependences on ω and u_* proposed for higher frequencies? Additional issues such as the effects of peak enhancement (Hasselmann et al. 1973) and Doppler distortion (Kitaigorodskii et al. 1975) in the frequency spectrum are also relevant and need to be included in the analysis.

In this contribution, the ensemble of available wavenumber data, together with the directional spreading function and frequency spectral form proposed by DHH, provides the basis for a model for $\Phi(k, \theta)$ for the fetch-limited growth of gravity wind waves above the spectral peak. This model is seen to be consistent with directional frequency observations and is then used to calculate reduced spectra in both wavenumber and frequency domains. The calculations presented here are aimed not only at demonstrating close conformity to existing observations in both domains, but also at isolating the underlying physical processes so as to obtain a better understanding of the structure of evolving wind wave spectra and the allied question of equilibrium ranges.

2. Analysis

For the frequency spectrum $F(\omega)$ and its associated directional frequency spectrum $G(\omega, \theta)$, a directional spreading function $h(\theta; \omega)$ exists such that $G(\omega; \theta) = h(\theta; \omega)F(\omega)$. It follows that $\xi^2 = \int_0^\infty F(\omega)d\omega = \int_0^\infty \int_{-\pi}^{\pi} G(\omega, \theta)d\theta d\omega = \int_0^\infty F(\omega) \int_{-\pi}^{\pi} h(\theta; \omega)d\theta d\omega$ and therefore $\int_{-\pi}^{\pi} h(\theta; \omega)d\theta = 1$. There is a direct parallel with this in the wavenumber domain involving the directionally averaged wavenumber spectrum $f(k)$, but for the present purpose it is not convenient to use this form but rather the component $\Phi(k, \theta_{\max})$ of the directional wavenumber spectrum in the direction $\theta_{\max}$ of the dominant wind waves at the spectral peak. Donelan et al. show that $\theta_{\max}$ need not be aligned with the wind direction, which results in a spectral dependence on the effective windspeed $U \cos\Omega$ rather than U, where Ω is the angle between the dominant waves and the mean wind. An alternative spreading function $D(\theta; k)$ is defined by

$$D(\theta, k) = \Phi(k, \theta)/\Phi(k, \theta_{\max}) \qquad (2.1)$$

which is not required to have unity polar integral, but is constrained only by the total wave energy requirement that

$$\int_{-\pi}^{\pi} \int_0^\infty \Phi(k, \theta_{\max})D(\theta, k)kdkd\theta = \overline{\xi^2}.$$

The two spreading functions $h(\theta; \omega)$ and $D(\theta; k)$ have different relative magnitudes, but their directional dependence is the same. It is also useful to recall the relationship of $\Phi(k, \theta)$ to the frequency spectrum $F(\omega)$ and to the directional frequency spectral slice $G(\omega, \theta)$, as detailed by Phillips (1977, §4.1):

$$F(\omega) = \int_{-\pi}^{\pi} G(\omega, \theta)d\theta$$

$$= 2g^{-1/2} \int_{-\pi}^{\pi} [k^{3/2}\Phi(k, \theta)]_{k=\omega^2/g}d\theta. \qquad (2.2)$$

From (2.1), the polar component of the directional wavenumber spectrum $\Phi(k, \theta)$ in any direction θ is given by

$$\Phi(k, \theta) = \Phi(k, \theta_{\max})D(\theta; k). \qquad (2.3)$$

Formulation of the wavenumber spectral model

Throughout this paper, the focus is on fetch-limited wind wave growth. Apart from the relative lack of complexity in relation to more general wind wave situations, most of the available wavenumber spectra and complementary frequency spectra were obtained under fetch-limited conditions. The applicability to more general situations is taken up in the discussion.

Figure 1 shows one-dimensional spectra $\phi(k_i)$ from several investigations for conditions closely approximating fetch-limited growth: the high wavenumber data of Banner et al. (1989); the lower wavenumber $\phi(k_1)$ spectra (the wind is in the one-direction) of Schule et al. (1971) and Barnett and Wilkerson (1967) for a succession of fetches; the high windspeed, very long peak wavelength data calculated from Run 36/1 in Jackson et al. (1985a). This interesting run approximated fetch-limited conditions until several hours before the spectrum was measured, when the wind direction began turning gradually, initiating a second spectral peak directed from the original wind wave system by about 90°. According to the sudden wind shift computations of Young et al. (1987), some degree of attenuation of the original wind sea might have occurred. The apparent consistency between the wavenumber dependence of the spectral range just above the spectral peak wavenumbers for all these one-dimensional spectra in the dominant wave direction over

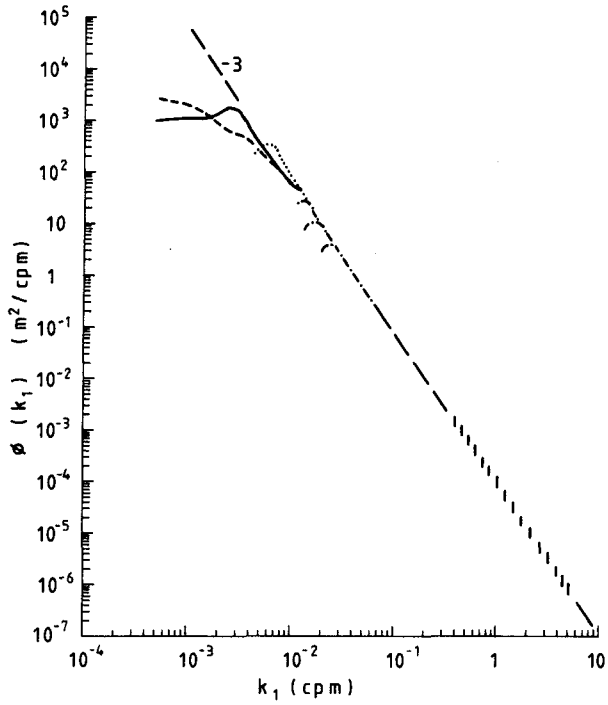

FIG. 1. One-dimensional wavenumber spectra $\phi(k_1)$ in the wind direction for fetch-limited wind wave growth conditions. (Solid) Jackson et al. (1985a, Run 36/1); (dot-dash) Schule et al. (1971); (dotted) Barnett and Wilkerson (1967); (hatched) Banner et al. (1989). Also shown: (short dash) Jackson et al. (1985a), orthogonal $\phi(k_2)$ spectrum. The background asymptote shown (long dash) has slope k_1^{-3}.

such a wide range of dominant wavelengths is noteworthy. Also, the Jackson et al. 1985a) Run 36/1 transverse spectrum reflects the strong directionality of the wave field near the spectral peak. It is seen that the transverse spectrum has less energy near the spectral peak, a lower spectral slope and only begins to asymptote to the dominant wave direction spectrum for $k/k_p > O(4)$. These directional aspects are better understood from the directional wavenumber spectrum $\Phi(k, \theta)$, which allows a basic understanding of the form of observed reduced wavenumber and frequency spectra.

Using the transform relationship (2.2) and the wave age dependence in the frequency spectrum (1.13) proposed by DHH, together with the wave age-independent form of spreading function found by DHH [see (2.8) and (2.9) below], the available wavenumber spectral data supports the form of the two-dimensional wavenumber spectral density slice in the dominant wave direction:

$$\Phi(k, \theta_{\max}) = 0.45 \times 10^{-4}(U/c_p)^{1/2}k^{-4} \quad (k \text{ in cpm}). \quad (2.4)$$

Underlying the determination of (2.4) from observed wavenumber spectra $\Phi_s(k, \theta)$ is the use of a plausible directional spreading function $D(\theta; k)$. Three forms for $D(\theta; k)$ are considered here: the form proposed by DHH, which needs to be extrapolated to higher wavenumbers, and those reported by Hasselmann et al. (1980) and Mitsuyasu et al. (1975), for the case of fetch-limited growth conditions. The relative merits of these different spreading functions are discussed critically in DHH, and it is apparent that basic problems still remain with the determination of this fundamental quantity, particularly for wave components well above the spectral peak.

Mitsuyasu et al. (1975) and Hasselmann et al. (1980) both proposed

$$D(\theta, k) = \cos^{2s}[(\theta - \theta_{\max})/2] \quad (2.5)$$

with different dependences of the spread exponent s on two underlying parameters: the dimensionless wavenumber k/k_p and the wave age c_p/U of the spectral peak. Based on pitch-and-roll buoy data, Mitsuyasu et al. (1975) proposed

$$s = 11.5(c_p/U)^{2.5}(k/k_p)^{-1.25} \quad \text{for} \quad k/k_p > 1, \quad (2.6)$$

while Hasselmann et al. (1980) proposed

$$s = 9.77(k/k_p)^{-[0.32+0.72/(c_p/U)]} \quad \text{for} \quad k/k_p > 1. \quad (2.7)$$

On the basis of radar backscatter measurements, McLeish and Ross (1983) suggested that actual directional distribution widths may be narrower than those reported from pitch-and-roll buoy determinations. This was confirmed by DHH using a wave probe array. Donelan et al. examined two alternate forms for $D(\theta, k)$: the form (2.5) and one based on the form

$$D(\theta; k) = \operatorname{sech}^2 b(\theta - \theta_{\max}) \quad (2.8)$$

with the width parameter $b(k)$ as discussed below. Based on wavenumber–frequency spectral techniques with an improved angular resolution over pitch-and-roll buoy data spreading estimates, DHH found significant differences arising from noise limitations, depending on the choice of fitting the full angular distribution or the half-power points. The latter reduced tail noise influence and suppressed the wave age dependence found by the previous investigators. The DHH determination of $D(\theta, k)$ only reached $k/k_p \sim 2.6$ and is therefore restricted to the peak enhancement region. Above $k/k_p \sim 2.6$ considerable scatter developed in the measured $b(k)$, which was interpreted by DHH as a high wavenumber cutoff in the directional spreading function. However, a spreading cutoff at such low k/k_p is unlikely, a view supported by recent unpublished results (Donelan, personal communication) using an extension of the wave gauge array technique to higher wavenumbers, which show a continued increase in spreading beyond $k/k_p \sim 2.56$ with a spreading cutoff at much shorter scales, consistent with the broad di-

rectional distribution observed by Banner et al. (1989) at higher k/k_p. On this basis, extrapolation of the DHH spreading distribution found near the spectral peak to higher wavenumbers, including the expected gravity equilibrium subrange, is proposed according to the form (2.9b), for which further support follows from a comparison of predicted and observed frequency spectra. Based on the half-power fitting criterion, the form for $D(\theta; k)$ adopted here is (2.8) with

$$b = \begin{cases} 2.28(k/k_p)^{-0.65}, \\ \quad \text{for} \quad 0.97 < k/k_p < 2.56 \quad (2.9a) \\ 10^{-0.4+0.8393\exp[-0.567\ln(k/k_p)]}, \\ \quad \text{for} \quad k/k_p > 2.56. \quad (2.9b) \end{cases}$$

The form for (2.9b) simply matches the ordinate and slope of (2.9a) at the transition $k/k_p = 2.56$ and provides a suitable spreading cutoff at high wavenumbers. These directional spreading characteristics for different k/k_p values are shown in Fig. 2a. The corresponding folded form $D_s(\theta; k)$, arising from frozen spatial image wavenumber spectral determinations, is given by

$$D_s(\theta; k) = 0.5[D(\theta; k) + D(\theta - \pi, k)] \quad (2.10)$$

and is shown for reference in Fig. 2b.

Near the spectral peak, reference to Fig. 2 shows that to a close approximation,

$$\Phi(k, \theta_{\max}) \sim 2\Phi_s(k, \theta_{\max}). \quad (2.11)$$

At higher wavenumbers, this approximation is slightly degraded, owing to the assignment of a small proportion of rearward-traveling wave energy by the choice of spreading model.

The high wavenumber $\Phi_s(k)$ findings of Banner et al. (1989) were transformed using (2.8) and (2.9b), giving

$$\Phi(k, \theta_{\max}) \sim 0.5 \times 10^{-4} k^{-4}. \quad (2.12)$$

It is noted here that a higher wavenumber cutoff in the spreading function, which would produce broader directionality for the high wavenumbers, would have the effect of slightly reducing the coefficient in (2.12): a truly isotropic directional distribution would result in a coefficient of 0.3×10^{-4} in (2.12).

The available data on $\Phi(k, \theta_{\max})$, extracted using (2.9) from Jackson et al. (1985a, run 36/1) and from Holthuijsen (1983) together with $\Phi(k, \theta)$ derived from Banner et al. (1989) are shown in Fig. 3a, weighted by k^4 and $(U/c_p)^{-1/2}$, which shows consistent support for the proposed form (2.4) over a considerable range of peak wavenumbers, excluding the noisy tail regions. The slight reduction in spectral level reflected in the Jackson et al. (1985a) data was possibly associated with attenuation caused by turning winds, as discussed earlier. The classic SWOP data (Cote et al. 1960) were also analyzed, but are not included here with the fetch-limited growth data. Interestingly, for the SWOP data, $\Phi(k, \theta_{\max})$ was found to conform to k^{-4} dependence, but with a spectral level low by a factor of O(2), as noted previously by others (e.g., Phillips 1977, §4.5). A detailed discussion of these aspects of the SWOP spectrum is given by McLeish and Ross (1985) and

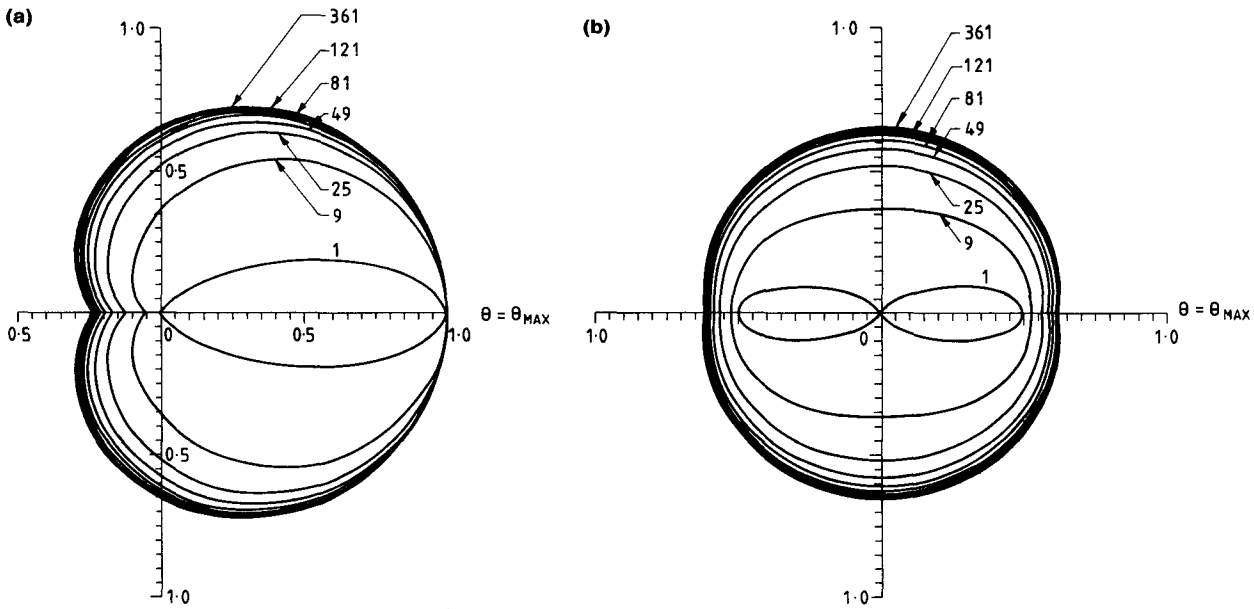

FIG. 2. (a) Polar plot of the DHH (Donelan et al. (1985) directional spreading function $D(\theta; k)$ given by (2.8) and (2.9), shown for the various indicated k/k_p values. (b) As in (a), but showing the equivalent spreading function $D_s(\theta; k) = 0.5[D(\theta; k) + D(\theta - \pi, k)]$ as observed in a purely spatial domain measurement.

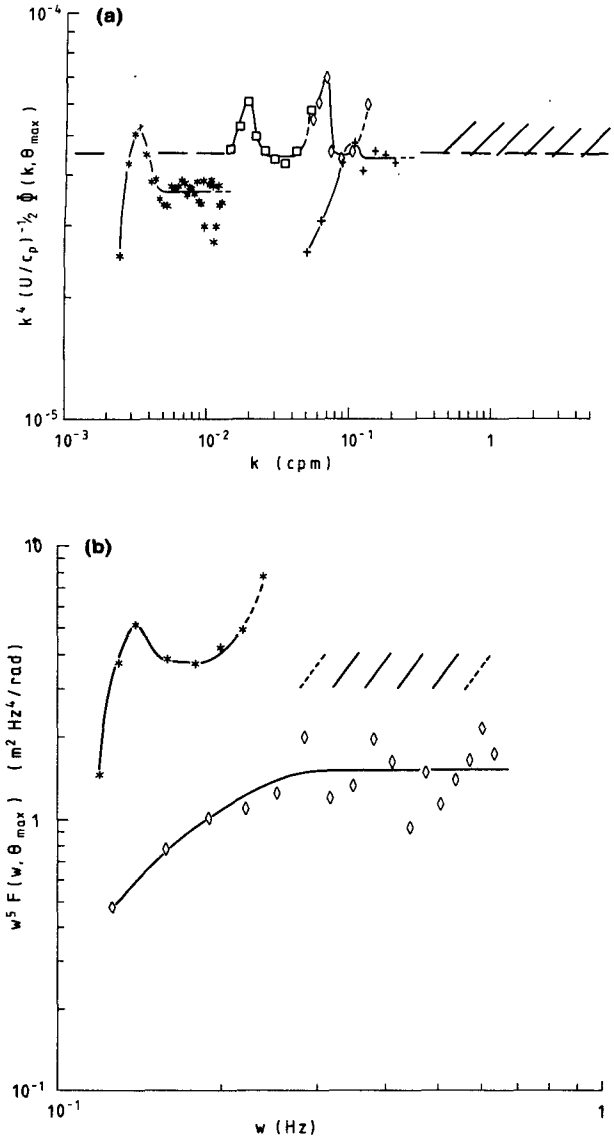

FIG. 3. (a) Directional wavenumber spectral slice $\Phi(k, \theta_{max})$ in the dominant wave direction for fetch-limited wave growth conditions, shown weighted by k^4 and $[U/c_p]^{-1/2}$. *: Jackson et al. (1985a, Run 36/1), +: Holthuijsen (1983, Obs.#1), ◇: Holthuijsen (1983, Obs.#2), □: Holthuijsen (1983, Obs.#4). ///: Banner et al. (1989), with assumed $D(\theta; k)$ according to (2.10) and (2.11). Background asymptote shown (long dash) has spectral level 0.45×10^{-4}. (b) Directional frequency spectral slice $G(\omega, \theta_{max})$ in the dominant wave direction for fetch-limited growth conditions, shown weighted by ω^5. *: Ewing (1969), ◇: Longuet-Higgins et al. (1963), ///: Donelan (private communication).

further consideration of the SWOP spectrum is given in section 4.

The model for the wavenumber spectrum adopted in this study is based on the observed data for $\Phi(k, \theta_{max})$, as fitted by (2.4) in conjunction with a plausible directional spreading function $D(\theta; k)$ and takes the form:

$$\Phi(k, \theta) = 0.45 \times 10^{-4} (U/c_p)^{1/2} k^{-4} D(\theta; k). \quad (2.13)$$

For typical k_p for ocean wind waves, this is in very close agreement with the form (1.17) derived from the DHH results on the basis of $D(\theta; k)$ given by (2.8) with (2.9a). The differences, whose magnitude is in the noise level of the observations, is of little consequence to the main conclusions of this study, and its effect on the reduced spectra is masked by uncertainties in $D(\theta; k)$.

Observational frequency domain support for the dependences in (2.13) is also available, from the slice through the directional frequency spectrum $G(\omega, \theta)$ in the dominant wave direction θ_{max}. Here, a transformation of (2.13) to give $G(\omega, \theta)$ according to the relationship expressed in (2.2) gives

$$G(\omega, \theta_{max}) \sim (U/c_p)^{1/2} \omega^{-5}. \quad (2.14)$$

Again, the availability of such data is limited and the accuracy of the spectral level depends on the amount of smoothing used in the spreading function determination. Nevertheless, observational evidence for the ω^{-5} frequency dependence in (2.14) for fetch-limited growth conditions is available in the $G(\omega, \theta)$ data of Longuet-Higgins et al. (1963, Record 10) and of Ewing (1969, Record 5), which are shown weighted by ω^5 in Fig. 3b. The lower spectral level in the former appears due to systematically broader directional widths, possibly reflecting different smoothing of the directional distributions. Donelan (personal communication) confirms ω^{-5} dependence for $G(\omega, \theta_{max})$ in very recent (unpublished) observations, with a spectral level in the weighted spectrum comparable with Ewing's record 5, as indicated on Fig. 3b. Each of these studies reveal ω^{-4} dependence for the frequency spectrum $F(\omega)$ near the spectral peak.

Finally, it should be noted that in the immediate neighborhood of the spectral peak (say $|k/k_p - 1| < 2$), a peak enhancement is to be expected, reflecting the slope of the waves at the spectral peak and, therefore, dependence on the dimensionless fetch xg/u_*^2, just as with the frequency spectrum (e.g., see Hasselmann et al. 1973; DHH). However, only the influence of peak enhancement on the high frequency part of the spectrum is considered in this study (§3c, §3d, §3e).

Section 3 describes the results of calculations of the one-dimensional wavenumber and frequency spectral forms that result from appropriate tranformations of the proposed model for the directional wavenumber spectrum (2.13), using a plausible form for the directional spreading function $D(\theta; k)$.

3. Results

a. *Reduced wavenumber spectra*

The one-dimensional spectrum in the dominant wave direction $\phi(k_1)$ was calculated for the gravity range above the peak enhancement region $k/k_p \sim 2$.

The transverse one-dimensional spectrum $\phi(k_2)$ requires knowledge of the entire spectral shape including the spectral peak and below, and is not included here.

The integration (1.4) using the proposed directional wavenumber spectrum (2.13) with any of the different spreading distribution functions described in section 2a does not have a straightforward analytic form over the spectral subrange of interest, necessitating numerical computation. The wavenumber and windspeed dependences for $\phi(k_1)$ were computed for typical ocean wave and wind conditions, assuming the linear dispersion relation to relate peak frequency and peak wavenumber: 6 second waves ($k_p = 0.0148$ cpm) and 12 m s^{-1} windspeed, for which $U/c_p \sim 1.28$. The effect of doubling and halving the windspeed at the same fetch, under fetch-limited growth conditions, was also investigated using the fetch-limited relationship proposed by DHH [their Eq. (5.5)] to calculate the cor-

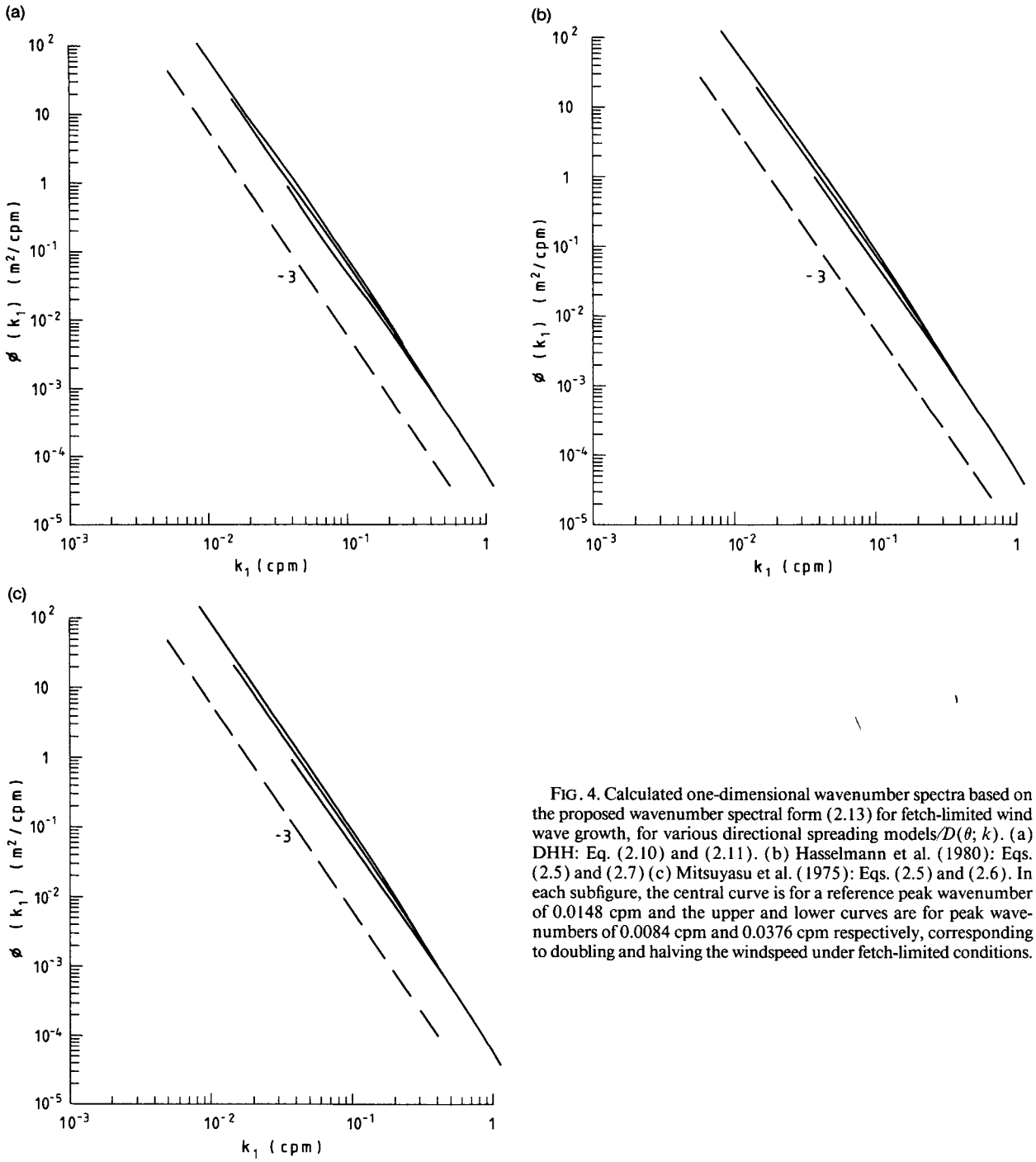

FIG. 4. Calculated one-dimensional wavenumber spectra based on the proposed wavenumber spectral form (2.13) for fetch-limited wind wave growth, for various directional spreading models $D(\theta; k)$. (a) DHH: Eq. (2.10) and (2.11). (b) Hasselmann et al. (1980): Eqs. (2.5) and (2.7) (c) Mitsuyasu et al. (1975): Eqs. (2.5) and (2.6). In each subfigure, the central curve is for a reference peak wavenumber of 0.0148 cpm and the upper and lower curves are for peak wavenumbers of 0.0084 cpm and 0.0376 cpm respectively, corresponding to doubling and halving the windspeed under fetch-limited conditions.

responding peak wavenumbers. For $U = 24$ m s^{-1}, the corresponding peak wavenumber is 0.0084 cpm, with $U/c_p \sim 1.76$, while for $U = 6$ m s^{-1}, $k_p = 0.0376$ cpm and $U/c_p \sim 0.93$. The calculated $\phi(k_1)$ for the different spreading function models are shown in Figs. 4a–c. From these results, it is seen that for each of the proposed directional spreading models, the predicted wavenumber dependence for $\phi(k_1)$ is close to k_1^{-3}, which is in agreement with the observed one-dimensional wavenumber spectra in Fig. 1. The wavenumber dependence of the calculated spectra differs from the $k_1^{-2.5}$ variation predicted by (1.15) and the calculated windspeed dependence is significantly weaker than the linear variation according to (1.15).

A straightforward calculation establishes the form of the omnidirectional wavenumber spectrum $\bar{\phi}(k)$ for (2.13) with DHH spreading (2.11). The integral (1.5) for $\bar{\phi}(k)$ takes the form, with $\theta_{\max} = 0$,

$$\bar{\phi}(k) = 0.45 \times 10^{-5}(U/c_p)^{1/2}k^{-3}\int_{-\pi}^{\pi} \operatorname{sech}^2(b\theta)d\theta$$

$$= 0.9 \times 10^{-5}(U/c_p)^{1/2}k^{-3}b^{-1}\tanh(b\pi) \quad (3.1)$$

where b is given by (2.9). Above the peak enhancement region, where (2.9a) applies, b decreases according to (2.9b) as the directional spreading broadens. For b sufficiently large, i.e. $b > 1$, $\tanh(b\pi) \sim 1$ and (2.9b) indicates that this holds out to about $k/k_p \sim 3.7$, for which (3.1) gives

$$\bar{\phi}(k) \sim (U/c_p)^{1/2}k_p^{-0.65}k^{-2.35}. \quad (3.2a)$$

For very large k/k_p, the spreading cutoff in (2.9b) gives a constant value of $b \sim 0.4$, for which the corresponding high wavenumber form for $\bar{\phi}(k)$ is $\bar{\phi}(k) \sim (U/c_p)^{1/2}k_p^{-0.65}k^{-3}$. Similarly, for large k/k_p, the directionally averaged wavenumber spectrum has the form

$$f(k) \sim (U/c_p)^{1/2}k_p^{-0.65}k^{-4}. \quad (3.2b)$$

A calculation of $\bar{\phi}(k)$ for the reference conditions quoted above is shown in Fig. 5a. For the energy containing subrange $2.5 < k/k_p < 10$, this shows a predicted behavior of $\bar{\phi}(k) \sim k^{-n}$ with $n \sim 2.5$. $\bar{\phi}(k)$ extracted from the Jackson et al. (1985a) Run 36/1 data gives the omnidirectional spectrum plotted in Fig. 5b, similar to (3.3). It is noted that this wavenumber dependence near the spectral peak results from the k/k_p dependence of the azimuth-averaged directional spreading function.

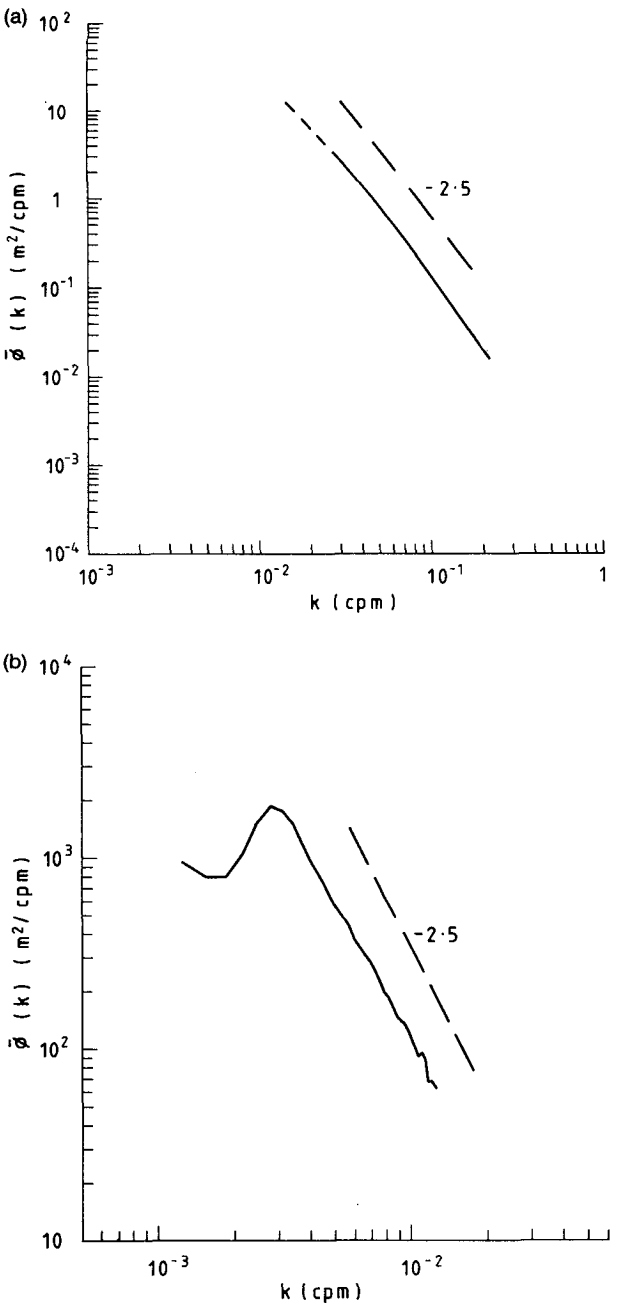

FIG. 5. Omnidirectional wavenumber spectra near the spectral peak. (a) calculated from (2.13) using (2.8) and (2.9) for $k_p = 0.0148$ cpm and $U/c_p = 1.28$. The region at the spectral peak where peak enhancement is operative is shown (dashed). (b) Extracted from the data of Jackson et al. (1985a, Run 36/1).

b. *The effect of directional spreading on calculated frequency spectra*

The influence of the directional spreading alone on the frequency spectrum is determined from (2.2) using (2.13) and the linear dispersion relation, with the aim of determining the predicted frequency and the apparent windspeed dependences. Peak enhancement effects are not included here. The resulting form for $F(\omega)$ is

$$F(\omega) = 0.9 \times 10^{-4}g^2(U/c_p)^{1/2}\omega^{-5}\left[\int_{-\pi}^{\pi} D(\theta; k)d\theta\right]_{k=\omega^2/g}. \quad (3.3)$$

Note that the dispersion relation $\omega^2 = gk$ does not allow for local Doppler effects due to direct wind influence and dominant wave orbital motions, which are examined subsequently.

An analysis similar to that for the reduced wavenumber spectra in section 3a was carried out to examine the sensitivity of the shape of the frequency spectra which arise from the proposed spectral form (2.13) using the different spreading distributions $D(\theta; k)$ described above, noting particularly the predicted dependence on frequency and on the windspeed.

For the DHH spreading distribution, (3.3) with $\theta_{max} = 0$ gives

$$F(\omega) = 0.90 \times 10^{-4} g^2 (U/c_p)^{1/2} \omega^{-5} b^{-1} \int_{-\pi}^{\pi} \operatorname{sech}^2(b\theta) d\theta. \quad (3.4)$$

The same considerations as discussed for $\bar{\phi}(k)$ apply here. For DHH spreading, just above the peak enhancement region, out to $\omega/\omega_p \sim 2$ (corresponding to $k/k_p \sim 4$), $b \sim (\omega/\omega_p)^{-1.3}$ and so (3.4) yields

$$F(\omega) \sim (U/c_p)^{1/2} \omega_p^{-1.3} \omega^{-3.7} \quad (3.5a)$$

for this frequency subrange. For large $\omega/\omega_p \sim 20$–30, the spreading cutoff gives $b \sim 0.4$ and (3.4) gives the form

$$F(\omega) \sim (U/c_p)^{1/2} \omega_p^{-1.3} \omega^{-5} \quad (3.5b)$$

for high frequencies relative to the spectral peak.

From (3.2) and (3.5) it may be seen that the explicit windspeed dependence at a fixed fetch can be calculated from the resultant c_p and k_p dependence on windspeed and fetch, e.g., Eq. (5.5) in DHH which proposes $U_c/c_p \sim (xg/U_c^2)^{-0.23}$, where x is the fetch. Taking the ideal case $U_c = U$, then this relation gives $c_p \sim U^{0.54}$, $\omega_p \sim U^{-0.54}$ and $k_p \sim U^{-1.08}$ at a fixed fetch. With these DHH fetch dependencies, the predicted windspeed dependence in (3.2) and (3.5) is $U^{0.93}$. Other authors have proposed different windspeed dependencies for $F(\omega)$, but this is very close to the linear correlation with U reported for many frequency spectral observations, such as those cited above [see (1.12)], especially in view of the potential errors in the empirical spreading exponent −0.65 in (2.9a).

For completeness, frequency spectra were calculated for the same representative peak wavenumbers and windspeeds used in section 3a, and the results plotted in Figs. 6a–c show the effect of doubling and halving the windspeed at a given fetch on the fetch-limited frequency spectrum components for the three different spreading function forms due to DHH, Mitsuyasu et al. (1975) and Hasselmann et al. (1980). The following major features are confirmed in each of these figures:

(i) the two different dependences on the frequency, ω^{-n} where $n \sim 4$ in the subrange $1.3 < \omega/\omega_p < 3$, transitioning at $\omega/\omega_p \sim O(3)$ to $n \sim 5$ towards higher ω/ω_p.

(ii) In the range $1.3 < \omega/\omega_p < O(3)$ where the $n \sim 4$ behavior is found, the calculated shifts in spectral level in Fig. 6a are seen to correspond fairly closely to a doubling and halving of the reference peak wavenumber spectral level, in accordance with the $U^{0.93}$ dependence calculated above. In Figs. 6b,c a near-linear dependence on U is also seen. Thus according to the model, only a small O(20%) part of the observed windspeed dependence in the frequency spectrum is due to the intrinsic windspeed dependence of $\Phi(k, \theta)$ via the term $(U/c_p)^{1/2}$, based on the variation of wave age with dimensionless fetch proposed by DHH [their Eq. (5.5)]. The major contribution arises from the variation of the directional spreading distribution with k/k_p (and wave age c_p/U, if applicable) as the spectral peak evolves, rather than to local growth through wind input. This viewpoint is consistent with that of several authors (e.g., Hasselmann et al. 1973; Komen et al. 1984; Young et al. 1987) who propose that the evolution of the peak, including the directional spreading distribution, is controlled mainly by the nonlinear spectral interactions near the spectral peak, rather than through direct wind action.

(iii) The results are generally qualitatively insensitive to the choice of $D(\theta; k)$: each of the directional spreading formulations reproduces frequency spectral trends which parallel the observations. It is evident that minor differences do exist, which have a secondary influence on the spectral slope and level. Their resolution awaits the refinement of the directional spreading formulations.

In summary, it has been shown that the proposed form (2.13) for the directional wavenumber spectrum for fetch-limited growth, in conjunction with any of the proposed wavenumber-dependent directional spreading formulations described above, gives predictions in the energy containing range [$1.5 < \omega/\omega_p < 3.5$] of (i) ω^{-n} behavior, with $n \sim 4$ (ii) an apparent near-linear dependence on the windspeed. Also, these calculations show a transition for higher ω/ω_p to ω^{-5}, with the transition point dependent on the rate at which $D(\theta; k)$ changes with k/k_p. For higher ω/ω_p, the measurements are either not available or continue at ω^{-n}, with n ranging from 3.3 to 5. The calculated ω^{-5} high frequency behavior found above needs to be reexamined in the light of possible Doppler shifting of the shorter waves by the orbital motions of the underlying dominant waves at the spectral peak and by wind drift and ambient currents. These aspects are investigated below in sections 3c–3e. Further support for the model near the spectral peak comes from a comparison of calculated and observed frequency spectra for those studies where wavenumber and frequency spectra were both measured, taken up in section 3f.

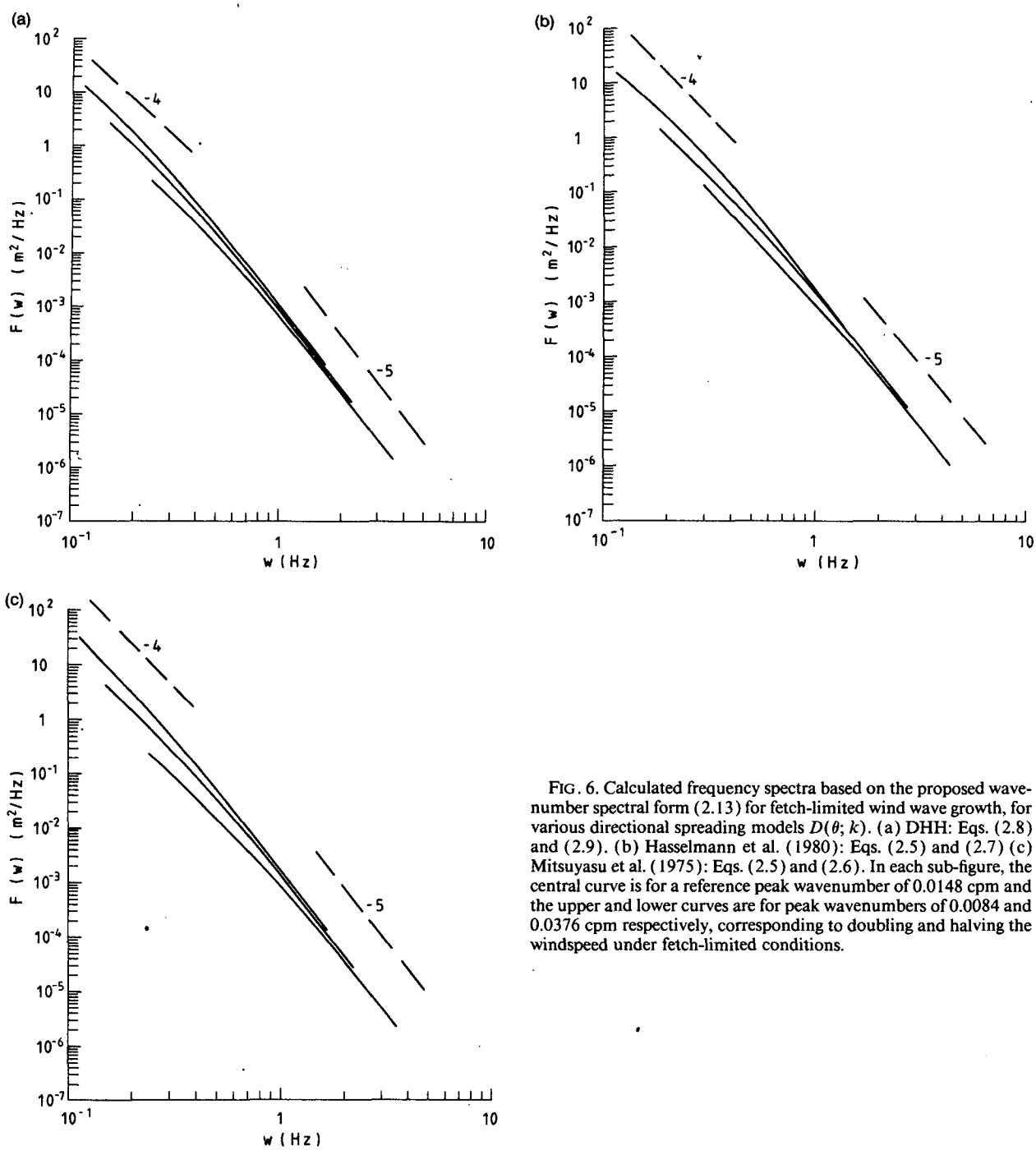

FIG. 6. Calculated frequency spectra based on the proposed wavenumber spectral form (2.13) for fetch-limited wind wave growth, for various directional spreading models $D(\theta; k)$. (a) DHH: Eqs. (2.8) and (2.9). (b) Hasselmann et al. (1980): Eqs. (2.5) and (2.7) (c) Mitsuyasu et al. (1975): Eqs. (2.5) and (2.6). In each sub-figure, the central curve is for a reference peak wavenumber of 0.0148 cpm and the upper and lower curves are for peak wavenumbers of 0.0084 and 0.0376 cpm respectively, corresponding to doubling and halving the windspeed under fetch-limited conditions.

c. *Effects of the slope of the spectral peak waves on calculated frequency spectra*

This section examines the influence of the slope of the spectral peak (or dominant) waves on the shape of the frequency spectrum. The additional effects of wind drift and ambient currents are investigated below. An exact calculation which addresses this problem is beyond our current capability and to illustrate the likely effects we have chosen a two-scale approximation calculation based on the kinematic conservation law (e.g., Phillips 1977, §2.6) and a short-wave energy modulation theory (e.g., Phillips 1981).

To calculate the net effect of the orbital motion of the spectral peak waves, the proposed wavenumber equilibrium spectral form (2.13), with $D(\theta; k)$ given

by (2.8) and (2.9), was modulated by an underlying long wave with a prescribed slope, corresponding to the spectral peak component which was assumed for simplicity to propagate in the direction θ_{max}. At a given phase of the long wave, the directional wavenumber spectrum was modulated in accordance with Phillips (1981) and transformed to a local frequency spectrum using the local orbital velocity in the dispersion relation: refraction effects were neglected as they were estimated to be of secondary importance. Phase averaging over the long wave then yielded the observed frequency spectrum, with negative apparent frequency components appropriately folded back into the positive frequency spectrum $F(\omega)$. Realistic orbital velocities, especially for steeper long waves, were computed from an exact steady nonlinear wave formulation due to Fenton (1986). Also, it should be noted that the two-scale approximation requires a sufficient scale separation for the long-wave orbital velocity to be effectively uniform over several cycles of the short-wave components. This implies that the approximation is unlikely to be very accurate for spectral components with $k/k_p < O(10)$ [or $\omega/\omega_p < O(3)$], but for shorter spectral scales, the method should provide a valid assessment of the net effect on the frequency spectrum of the steepness (peak enhancement) of the spectral peak waves. The present calculations extend those reported in Banner et al. (1989) which did not include directional spreading effects.

The results are shown in dimensionless form in Fig. 7 for a range of spectral peak wave slopes AK, where A is the amplitude and $K\ (=k_p)$ is the wavenumber of the spectral peak. For the present purpose, it is consistent with the two-scale approximation to estimate AK from the integrated height spectrum from $0.5\omega_p$ to $1.5\omega_p$, denoted by ξ_p^2 and use $AK \sim \sqrt{2}(\xi_p^2)^{1/2}k_p$. The calculation indicates that the spectral range $\omega/\omega_p < 3$ is relatively unaffected, but with increasing ω/ω_p, the effects of orbital motion Doppler shifting progressively increase the exponent of the frequency dependence from -5 to $-n$, where $n < 5$, with this exponent decreasing both with increasing frequency and stronger spectral peak enhancement. This effect is entirely kinematic and is independent of direct wind influence, and depends solely on the slope of the spectral peak waves, which is related to the wind through the dependence of the peak enhancement factor on the dimensionless fetch (e.g., Hasselmann et al. 1973; DHH). For typical open-ocean conditions, slopes $AK \sim 0.1$ are common, and a high frequency dependence of $\omega^{-4.5}$ is predicted for the gravity regime. For young waves under active growth conditions, $AK \sim 0.15$ to 0.2 is typical and a $\omega^{-3.8}$ high frequency dependence is predicted. For vanishingly small slopes of the modulating long waves, an asymptotic ω^{-5} limit is recovered. Thus, a clear source of departure from ω^{-5} dependence of the gravity wave regime arises from the net kinematic Doppler shifting influence of the orbital motion of the dominant waves.

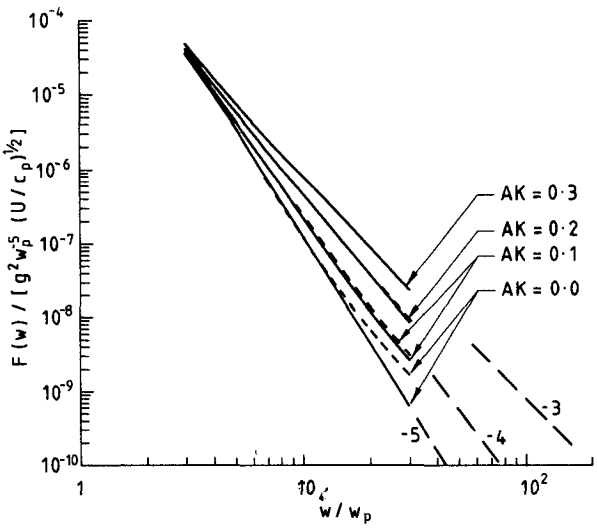

FIG. 7. Effect of the slope AK of the spectral peak on the tail of the frequency spectrum over $3 < \omega/\omega_p < 30$ for various indicated slopes AK of the spectral peak, due to spectral peak orbital velocity effects, is shown (solid). Computations were based on (2.13) with (2.8) and (2.9); ω is in rad s^{-1}. The additional influence of a wind drift current of $0.05c_p$, where c_p is the phase speed of the spectral peak, is shown (dashed).

d. Additional effect of the wind drift current on calculated frequency spectra

Here we examine the relative importance of the direct wind effect in the form of a thin surface wind drift current in the direction of propagation of the spectral peak component. An average level $u_s \sim 0.5u_*$ (Wu 1975) was assumed as representative for the very short gravity wind waves. Two additional physical considerations were included in the modeling of the drift current for the wavenumber range $9 < k/k_p < 900$ addressed by the calculation. First, advection by the wind drift current progressively reduces with decreasing wavenumber, as the associated orbital motions penetrate to increasingly greater depths where the wind drift is attenuated. This was modeled by assuming a variation in u_s from zero at $k/k_p = 1$ to an asymptotic level of $0.5u_*$ for $k/k_p = 900$ according to $u_s = 0.5u_*[1 - \text{sech}(0.01k/k_p)]$. Second, the modulating influence of the long wave on the surface drift current was included using a formulation due to Phillips and Banner (1974). These effects were included in the local dispersion relation.

Prior to carrying out the main body of computations, the computer code was checked by calculating the apparent frequency spectrum for a unidirectional wavenumber spectrum

$$\Phi(k, \theta) = \Phi(k, \theta_{max})\delta(\theta - \theta_{max})$$

with a superposed steady codirectional current, for which a simple analytical expression was derived. For

this test case, the computed and analytical results agreed closely.

Wind drift calculations were carried out for the same range of spectral peak slopes as in section 3c, taking $0.05c_p$ as the high wavenumber asymptotic value for u_s. For 6 second wind waves, this level is about 0.47 m s^{-1} and would correspond to a windspeed of about 26 m s^{-1}, based on typical neutral drag coefficient correlations (e.g., Wu 1980). The results of these calculations are shown in Fig. 7 in relation to the zero wind drift case and reveal that even for this strong generation case where $U/c_p \sim 2.8$, the additional influence of the wind drift current at higher frequencies in the gravity regime is small in comparison with orbital motion effects and reduces progressively as the spectral peak slope increases. It is also seen that the influence of the wind drift current decreases rapidly towards the energy-containing subrange closer to the spectral peak, where directional spreading was identified as the dominant influence shaping the frequency spectrum. For more moderate windspeeds and sea states, the influence of wind drift would be expected to be insignificant for this spectral subrange.

e. Additional effects of ambient ocean currents

The influence of an additional codirectional uniform ocean current field of strength $0.1c_p$ was calculated in the presence of a modulating spectral peak wave as in section 3c, again using a modified dispersion relation to include this additional source of Doppler shifting. The results, shown in Fig. 8, do not include wind drift effects. The incremental effect of a wind drift current (as in §3d) closely parallels the trends seen in Fig. 7 and is not shown here. Thus the overall effect of the codirectional current is an expected shift to higher spectral levels at any given frequency.

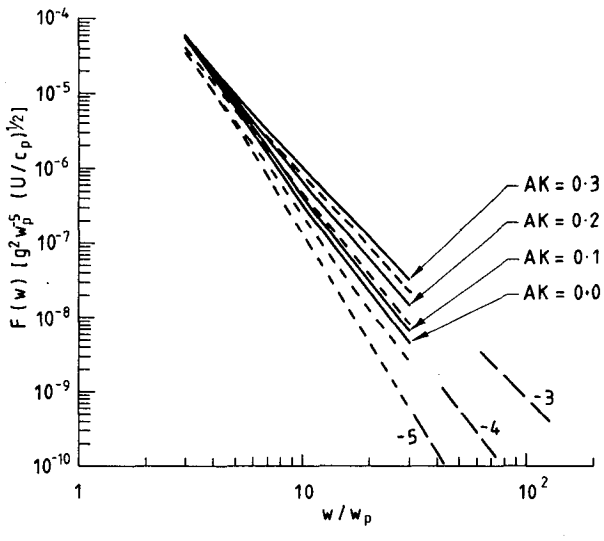

FIG. 8. As for Fig. 7, but showing the additional influence of an ambient codirectional current of $0.1c_p$, where c_p is the phase speed of the spectral peak. Wind drift effects are not included. The results for zero ambient current from Fig. 7 are shown (dashed).

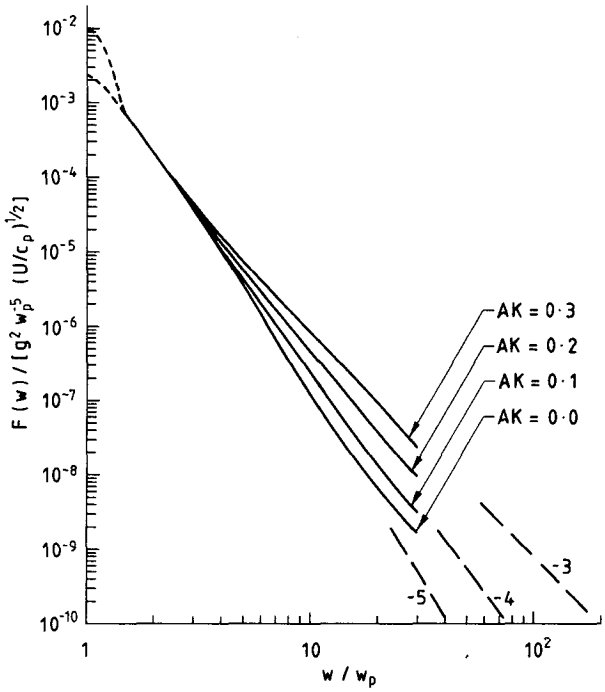

FIG. 9. Predicted composite frequency spectrum for the range $1.3 < \omega/\omega_p < 30$ from a synthesis of the results in Figs. 6 and 7. The conditions are as in Fig. 6, with a wind drift level as in Fig. 7. The ambient current is set to zero.

The results described in sections 3c–e indicate the relative strengths of the various kinematic Doppler distortion effects which can influence significantly the shape of the gravity regime of the tail of the frequency spectrum and which need to be considered in interpretations based on this class of measurements.

f. Comparison with observed wavenumber and frequency spectra

1) ONE-DIMENSIONAL WAVENUMBER SPECTRA

The observed one-dimensional wavenumber spectra $\phi(k_1)$ for fetch-limited situations shown in Fig. 1 conform closely to the proposed form

$$\phi(k_1) = A(U/c_p)^{1/2}k_1^{-3} \qquad (3.6)$$

which arises from the proposed model (2.13) with any of the forms for $D(\theta; k)$ in section 2a. A calculation using (2.8) and (2.9) for $D(\theta; k)$ gives $A \sim 0.6 \times 10^{-4}$, which corresponds closely to the spectral level $A \sim 0.6(\pm 0.2) \times 10^{-4}$ found from the observations.

2) FREQUENCY SPECTRA

A synthesis of the calculated frequency spectral behavior found in sections 3b, 3c and 3d provides the composite frequency spectrum shown in Fig. 9, which

combines the results from Figs. 6 and 7 into a unified dimensionless frequency spectral form for fetch-limited growth situations, applicable above the spectral peak. The dominant shaping influences near the spectral peak and for the tail have been described in detail above. It remains to compare this predicted composite form of the frequency spectrum with observed fetch-limited frequency spectra which cover all or part of the spectral range of interest.

(i) *Behavior near the spectral peak*

In the calculations that follow, the directional wavenumber spectral model (2.13) with the DHH form for $D(\theta; k)$ [(2.8), (2.9)] was transformed to frequency spectra for the wavenumber datasets where accompanying frequency spectra were observed. These cases were Jackson et al. (1989a, run 36/1), Holthuijsen (1981, obs 2) Banner et al. (1989, run 3). Results for these cases are shown in Figs. 10a–c from which it is seen that the calculated and observed frequency spectra are in close accord for the spectral range $1.3 < \omega/\omega_p < 3.5$, which excludes the peak enhancement region below $\omega/\omega_p \sim 1.3$. It should be noted that in Fig. 10a, the developing secondary wind sea peak at 0.1 Hz at 90° to the main wind sea was not taken into account in the model calculations and contributes to the underprediction of the tail energy level. Also in Fig. 10b the wind-wave system peaking at 0.31 Hz was superposed on a background low-frequency swell system.

We recall the anomalous frequency spectral behavior noted by Forristall (1981), who reported ω^{-4} depen-

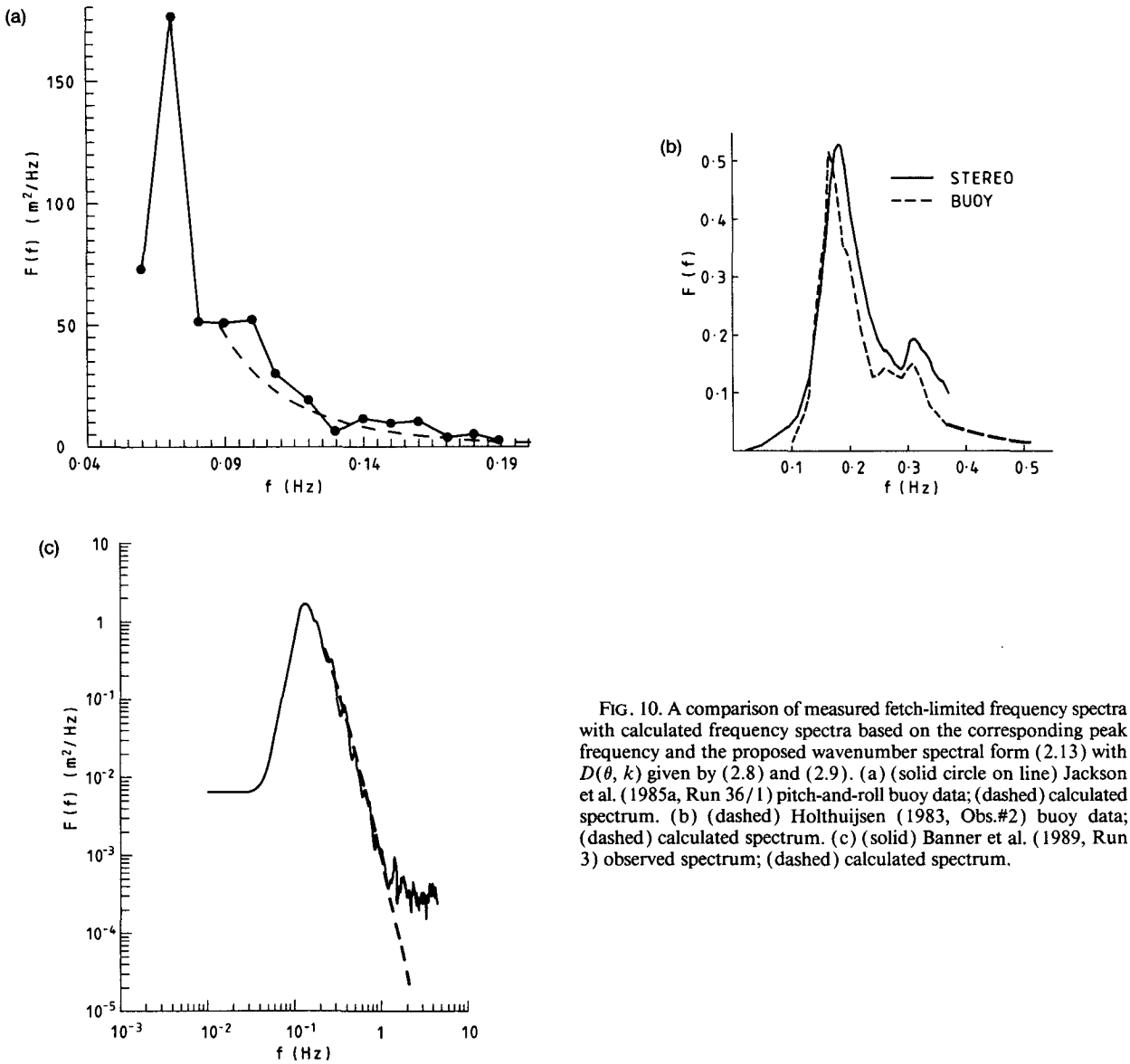

FIG. 10. A comparison of measured fetch-limited frequency spectra with calculated frequency spectra based on the corresponding peak frequency and the proposed wavenumber spectral form (2.13) with $D(\theta, k)$ given by (2.8) and (2.9). (a) (solid circle on line) Jackson et al. (1985a, Run 36/1) pitch-and-roll buoy data; (dashed) calculated spectrum. (b) (dashed) Holthuijsen (1983, Obs.#2) buoy data; (dashed) calculated spectrum. (c) (solid) Banner et al. (1989, Run 3) observed spectrum; (dashed) calculated spectrum.

dence for the range $1.5 < \omega/\omega_p < 3$ transitioning to ω^{-5} behavior above $\omega/\omega_p \sim 3$. This transitional behavior is predicted by the composite model calculations, provided the slope AK of the spectral peak is small. For the Forristall data, AK was around 0.08, for which a transition exponent of approximately −4.7 is predicted by the model, in close correspondence with Forristall's observations. This kind of spectral dependence might be expected generally for situations where the dimensionless fetch xg/u_*^2 is large, for which the slope of the spectral peak waves is reduced (e.g., Hasselmann et al. 1973; DHH) and the kinematic Doppler influence from the spectral peak waves does not appreciably distort the spectral range above $\omega/\omega_p > 3$ from ω^{-5} power law behavior.

(ii) *Behavior at high frequencies*

There have been relatively few studies of the higher frequency range of the spectrum because of reduced signal-to-noise ratio and operational difficulties in using the thinner wave probe wires in oceanic conditions. Here we consider the high frequency results reported by Mitsuyasu (1977) and Stolte (1984), which were found to conform closely to the fetch-limited relationships found by DHH. Calculated frequency spectra

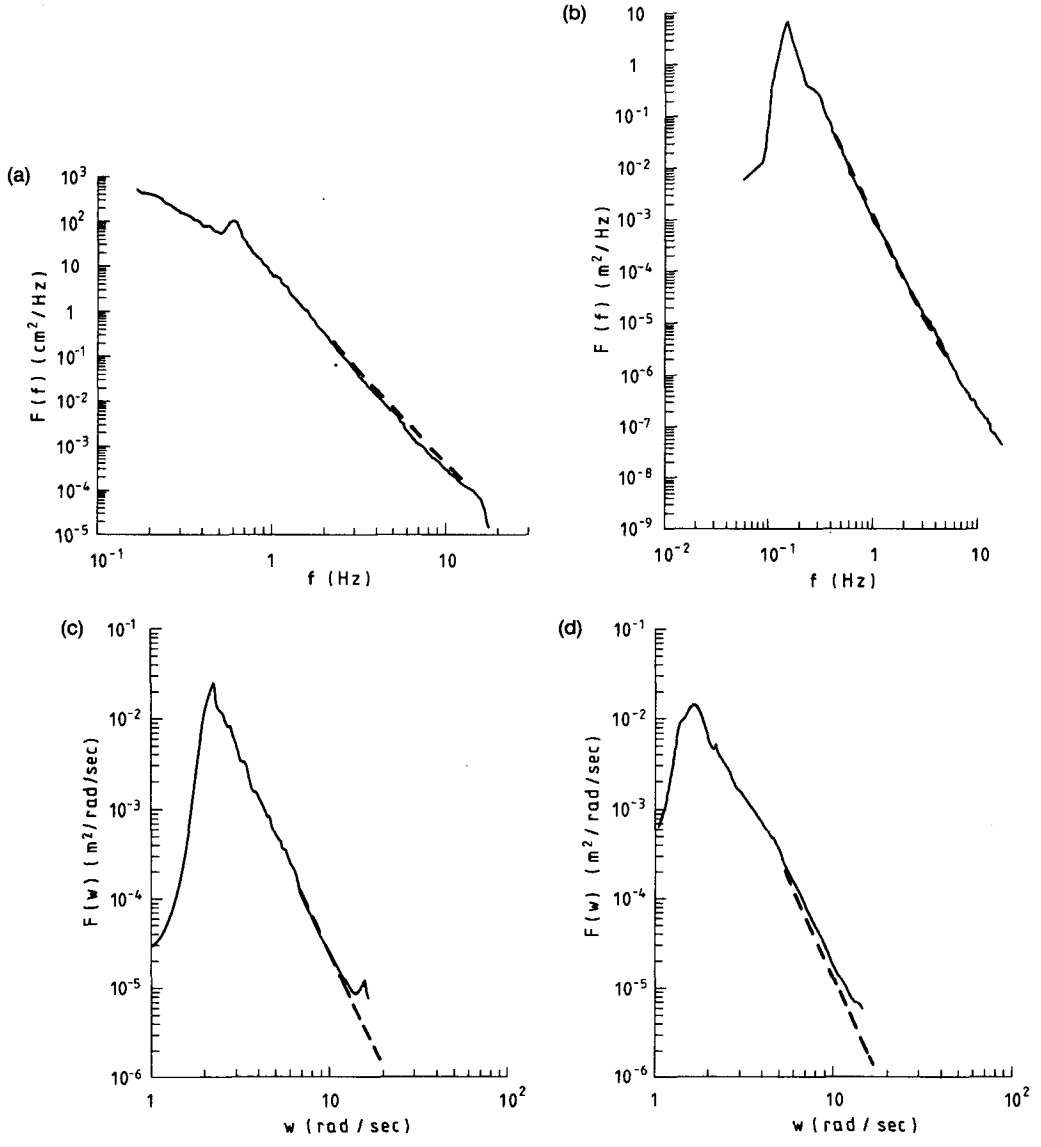

FIG. 11. Comparison of predicted and observed frequency spectra for higher frequencies $\omega/\omega_p > 3$. (a) Mitsuyasu (1977), $U/c_p \sim 3.0$, $\omega_p = 0.59$ Hz. (b) Stolte (1984), $U/c_p \sim 1.8$, $\omega_p = 0.15$ Hz. (c) DHH, $U/c_p \sim 3.6$, $\omega_p = 2.27$ rad s^{-1}. (d) DHH, $U/c_p \sim 1.0$, $\omega_p = 1.78$ rad s^{-1}. In each figure, the predicted spectrum is shown dashed.

based on the physical model, assuming DHH spreading, are shown superimposed on the observed frequency spectra in Figs. 11a,b. The spectral peak frequency, its slope and the wind drift level needed as input parameters for the model calculations were extracted from the data given in these papers. The frequency range was extended out to 30 times the spectral peak frequency for these calculations, but retaining only gravity in the dispersion relation. For intrinsic frequencies above about 7 Hz, the effects of surface tension are likely to influence the results, but this aspect was not pursued here due to lack of knowledge on the form of the wavenumber spectrum for the capillary–gravity wave regime and beyond. Although their frequency range is less extensive than those above, the frequency spectra shown by DHH in their Fig. 20 have also been included here in Figs. 11c,d, as they provide further examples of reliable fetch-limited data. Figure 11c is for $U/c_p \sim 3.6$ while Fig. 11d is for $U/c_p \sim 1.0$.

As can be seen in Fig. 11, the calculated and observed results are in close accord for each of the datasets examined here. It is also seen that a power-law exponent close to -4 provides a more reasonable fit to the observed spectra in the near-peak region than the -5 exponent originally proposed for this spectral region. It is evident that the form of extrapolation to high wavenumbers for $D(\theta; k)$ as expressed in (2.9b) has led to high-frequency spectral levels closely conforming to those observed, providing additional support for (2.9b). Other authors have reported frequency spectra extending out to high frequencies (e.g., Kondo et al. 1973; Leykin and Rozenberg 1984) and the calculated spectra corresponding to these observations were found to be in close agreement both near the spectral peak and for the higher frequencies in the gravity wide range.

Overall, for fetch-limited wind-wave growth situations, the proposed wavenumber spectral model is seen to provide close correspondence with the observed one-dimensional wavenumber and frequency spectra, both near the spectral peak and in the high frequency tail region. With this additional support for the underlying model, we address the implications of the model for identifying equilibrium spectral ranges and also its applicability to more general wind wave situations in section 4.

4. Discussion

Using the proposed model, we can address the question of equilibrium subranges and delineate their location more clearly. As before, we focus on fetch-limited growth and discuss the applicability to more complex situations at the end of this section.

For fetch-limited growth, eq. (1.10) for local spectral equilibrium requires that wave components in the equilibrium range should satisfy

$$\partial\Phi/\partial t + \mathbf{c}_g \cdot \nabla\Phi = c_{gx}\Phi_x \sim 0 \qquad (4.1)$$

i.e., spectral stationarity in the dominant wave direction. Before investigating how closely (4.1) is satisfied for the form of $\Phi(k, \theta)$ proposed here, we recall that $\Phi(k, \theta)$ has a narrow directional spectral peak region, which broadens towards higher k/k_p. Owing to the greater rate of change of directional spreading variation with k/k_p near the spectral peak, the spectral range $2.5 < k/k_p < 10$ is where (4.1) is least likely to be satisfied, for developing wave situations where the spectral peak evolves to lower wavenumbers with increasing fetch. A calculation was carried out to assess the order of magnitude of $c_{gx}\Phi_x$ in comparison to the magnitude of the wind input source term S_{in}, using the nondimensional peak frequency–fetch relation $U\omega_p/g = 11.6(xg/U^2)^{-1/4}$ together with the Snyder et al. (1981) form for the wind input source function and $\Phi(k, \theta)$ given by (2.13) with (2.8) and (2.9). The result is

$$c_{gx}\Phi_x/S_{in} = 2 \times 10^3 \times \frac{1.48(k_p/k)^{0.65}\theta \operatorname{sech}[2.28(k_p/k)^{0.65}\theta] - 0.125}{(k/k_p)^{1/2}(k_p x)(U\cos\theta/c_p - 1)} \qquad (4.2)$$

This result indicates that for $k = 4k_p$ in the dominant wave direction $\theta_{\max}$, the wind input source term is O(30) times larger than $c_{gx}\Phi_x$, so the equilibrium criterion is reasonably satisfied. However, for some of the $k = 4k_p$ wavenumber components oblique to the wind direction, $|c_{gx}\Phi_x/S_{in}|$ becomes comparable with the magnitude of this source term, indicating that these directional components are not close to equilibrium. Only when the downfetch evolution has approached full development (Pierson and Moskowitz 1964) will equilibrium conditions prevail for this spectral subrange, for which the angular spreading width must decrease if $F(\omega) \sim \omega^{-3}$ (Liu 1989) and (2.4) persists. Thus, while the spectrum is evolving with fetch, the spectral subrange near the peak is not in equilibrium, so that $\phi(k) \sim k^{-2.5}$, $\phi(k_1) \sim k^{-3}$ and $F(\omega) \sim \omega^{-4}$ subranges do not imply equilibrium for this region, in contrast to the viewpoint taken by Kitaigorodskii (1983), Phillips (1985) and others. Paradoxically, the shorter wave components, which are close to equilibrium in all directions (see Fig. 2a), transform to a frequency spectral form (as in Figs. 7–9), which appears to reflect nonequilibrium behavior in the frequency domain. This distortion arises from the kinematic Doppler shifting effects and appears to have confused previous assessments of equilibrium subranges.

In summary, equilibrium wind-wave spectral subranges are more perspicuous in the wavenumber spectral domain, which allows a consideration of the directional behavior of wave components unaffected by Doppler shifting. These equilibrium subranges are visualized in Fig. 12. Just above the spectral peak, the wavenumber components in the dominant wave direction are close to equilibrium, in contrast to the

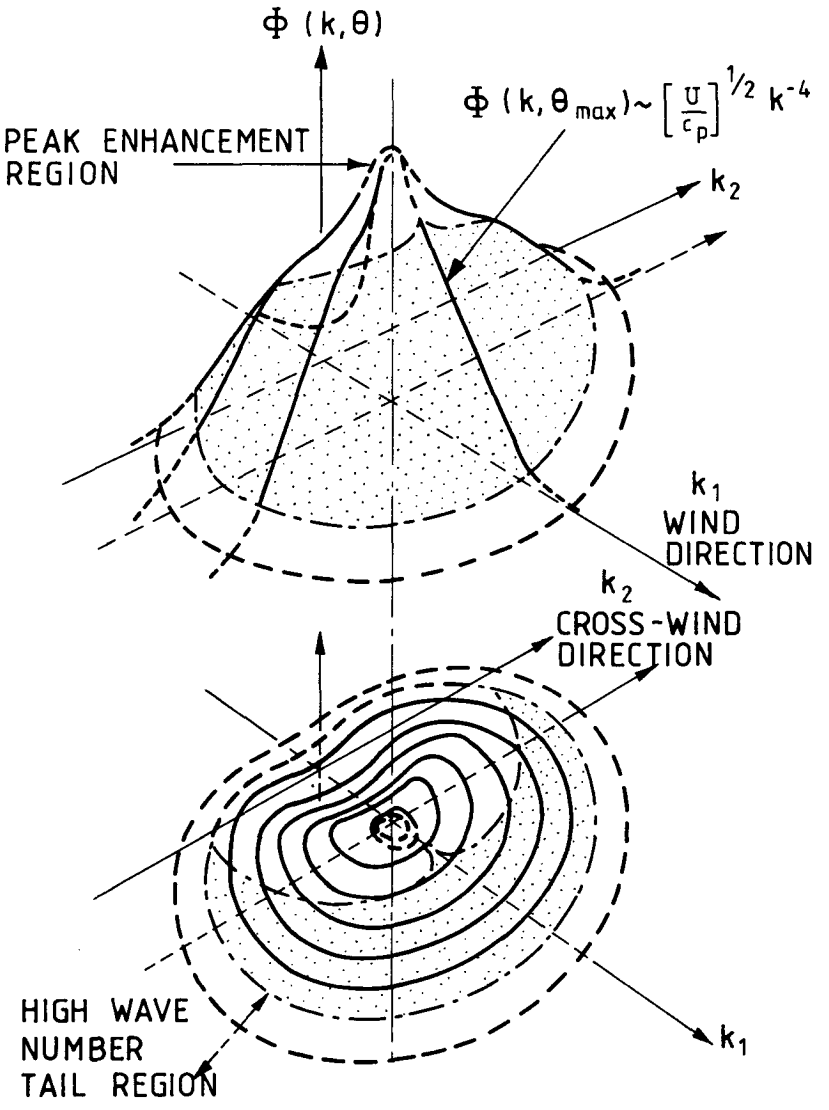

FIG. 12. Schematic diagram visualizing the directional wavenumber spectrum $\Phi(k, \theta)$ during fetch-limited wind wave growth. The axes are implicitly logarithmically scaled. The heavy straight line segment in the dominant wave (k_1) direction has the form (2.4) and the hatched zone indicates the envisaged equilibrium region.

oblique components for which equilibrium conditions are not satisfied. At higher wavenumbers in the gravity range, where the variation in $D(\theta; k)$ with k/k_p is small in all directions, equilibrium conditions prevail.

It remains an outstanding problem to understand the details of the spectral balance among the source terms that produce these equilibrium spectral dependences on wavenumber and wave age, and the corresponding spectral levels. This is left to a future study.

This section concludes with a brief discussion on the applicability of these results to other wind-wave growth situations. These might, for example, include duration-limited growth, turning wind situations, transiently growing and decaying winds and the presence of underlying shearing currents. According to McLeish and Ross (1985), the classical SWOP investigation belonged apparently to the last of these categories. The SWOP results had peak spectral levels well below that of standard fetch-limited conditions, as shown clearly by McLeish and Ross (1985). However, it is interesting to note that for the SWOP data, a detailed analysis indicates an apparent equilibrium wavenumber dependence for $\Phi(k, \theta_{max})$ of $0.3 \times 10^{-4} k^{-4}$ for the near-spectral peak region resolved by the stereophotogrammetric analysis. Again, the observed SWOP frequency spectrum could be recovered closely by a calculation such as in section 3f(2), but using this form for $\Phi(k, \theta_{max})$. However, in the light of the absence of any fur-

ther information on the mechanism(s) suppressing the energy of the SWOP spectrum below its fetch-limited level, it does not appear useful to pursue this further here. For these more general situations, including transient wind changes in strength and direction, it is likely that equilibrium conditions will still be satisfied for a subrange of high wavenumbers in the gravity regime. It would appear that numerical solution of the radiative transfer equation (e.g., Young et al. 1987) provides a path to future progress, once the outstanding problem of establishing a secure dissipation source function S_{diss} has been resolved. The proposed equilibrium form in the dominant wave direction may provide a useful basis for refining S_{diss}. Such investigations are currently in progress for fetch-limited and duration-limited growth, and should have potentially significant implications for numerical wave models in more general wind sea situations.

5. Conclusions

An empirically based physical model for fetch-limited wind wave growth has been proposed for the 2-D directional wavenumber spectral density in the dominant wave direction $\theta_{\max}$. It takes the form

$$\Phi(k, \theta_{\max}) = 0.45 \times 10^{-4}(U/c_p)^{1/2}k^{-4}$$

and appears to be applicable from short gravity-wave scales to very near the spectral peak. The directional wavenumber spectral density $\Phi(k, \theta)$ in any other direction is obtainable from

$$\Phi(k, \theta) = \Phi(k, \theta_{\max})D(\theta; k)$$

where the directional spectral function $D(\theta; k)$ reflects the decreasing directionality of the wave field with increasing wavenumber.

Further support for the proposed model derives from several aspects of predicted reduced wavenumber and frequency spectra calculated from this model, using a recent determination for $D(\theta; k)$ due to Donelan et al. (1985), plausibly extrapolated to higher wavenumbers, and the linear gravity-wave dispersion relation. Near the spectral peak, calculated one-dimensional and omnidirectional wavenumber spectra show dependences of k^{-3} and $k^{-2.5}$, respectively, in close correspondence with observed spectra. Calculated frequency spectra show a dependence near the spectral peak of close to ω^{-4}, arising primarily from the dependence of $D(\theta; k)$ on k/k_p, which also has a strong role in establishing the observed near-linear dependence on windspeed. Further from the spectral peak, the Doppler shifting due to orbital motions of the spectral peak waves plays a major part in influencing the spectral dependence of the intermediate and high frequency regions of the gravity wind-wave frequency spectrum. The high frequency tail is also affected by wind drift currents, which appear to have only a secondary influence that decreases as the spectral peak slope increases. Ambient ocean currents can also influence this spectral region and should be monitored during observational studies of high frequency wind-wave components. In addition, a composite model that embraces the two frequency spectral subranges just described predicts frequency spectra in close agreement with observed frequency spectra for fetch-limited growth situations, both near the spectral peak and for the high-frequency tail region in the gravity range.

Further observational wavenumber–frequency spectral determinations are needed to provide further direct confirmation and refinement of the model, particularly for wavenumbers k/k_p distant from the spectral peak, which constitutes a very considerable technical challenge. However, in its present form, the proposed model serves the important role of clarifying the previously elusive question of equilibrium spectral subranges. In this regard, it is found that near the spectral peak, equilibrium conditions prevail for wavenumber components in the dominant wave direction while lateral components are not in equilibrium. Thus, the energy-containing subrange just above the spectral peak, where $u_*\omega^{-4}$ frequency spectra are reported for fetch-limited growth before full development, is not an equilibrium subrange. This is contrary to previous interpretations. There is, however, an equilibrium subrange in the directional wavenumber spectrum for the higher gravity wavenumber components, which is masked in the frequency spectrum by Doppler influences from the orbital motion of the dominant waves and from wind drift and ambient currents.

The model also provides a useful test case for assessing models for the spectral dissipation source term by exploiting a previously unrecognized local equilibrium form in the dominant wave direction. The question of the detailed balances within the source terms in the governing radiative transfer equation, which lead to the form of the equilibrium spectral subrange structure proposed here, is left to a future study, as are the behavior of the spectral peak itself and of the technologically important very high wavenumber tail, where radar backscatter data suggest that a wind speed dependence is operative, whose strength appears to increase with increasing wavenumber.

Acknowledgments. The author gratefully wishes to acknowledge the following contributions: useful discussions with several colleagues during the course of this investigation, as well as helpful comments from the reviewers; the support provided for the author's ocean wavenumber spectral studies by the Australian Marine Science and Technology Grants Scheme and by the U.S. Office of Naval Research; the hospitality of the Ocean Sciences Group, Defence Science and Technology Organisation, where the author completed a first draft of this work while on leave.

REFERENCES

Banner, M. L., I. S. F. Jones and J. C. Trinder, 1989: Wavenumber spectra of short gravity waves. *J. Fluid Mech.*, **198,** 321–344.

Barnett, T. P., and J. C. Wilkerson, 1967: On the generation of ocean wind-waves as inferred from airborne radar measurements of fetch-limited spectra. *J. Mar. Res.*, **25,** 292–321.

Cote, L. J., J. O. Davis, W. Marks, R. J. McGough, E. Mehr, W. J. Pierson Jr., J. F. Ropek, G. Stephenson and R. C. Vetter, 1960: The directional spectrum of wind-generated sea as determined from data obtained by the stereo wave observation project. Meteor. Pap., New York University, College of Engineering, Vol. 2, No. 6, 88 pp.

Donelan, M. A., and W. J. Pierson, 1987: Radar scattering and equilibrium ranges in wind-generated waves with application to scatterometry. *J. Geophys. Res.*, **92,** 4971–5029.

——, J. Hamilton, and W. H. Hui, 1984: Directional spectra of wind-generated waves. *Phil. Trans. Roy. Soc. London,* **A315,** 509–562.

Ewing, J. A., 1969: Some measurements of the directional wave spectrum. *J. Mar. Res.*, **27,** 163–171.

Fenton, J. D., 1988: The numerical solution of steady water wave problems. *Comput. Geosci.*, **14,** 357–368.

Forristall, G. Z., 1981: Measurements of a saturated range in ocean wave spectra. *J. Geophys. Res.*, **86,** 8075–8084.

Hasselmann, D. E., M. Dunckel and J. A. Ewing, 1980: Directional wave spectra observed during JONSWAP 1973. *J. Phys. Oceanogr.*, **10,** 1264–1280.

Hasselmann, K., 1962: On the nonlinear energy transfer in a gravity wave spectrum. Part 1. *J. Fluid Mech.*, **12,** 481–500.

——, 1963a: On the nonlinear energy transfer in a gravity wave spectrum. Part 2. *J. Fluid Mech.*, **15,** 273–281.

——, 1963b: On the nonlinear energy transfer in a gravity wave spectrum. Part 3. *J. Fluid Mech.*, **15,** 385–398.

——, T. P. Barnett, E. Bouws, H. Carlson, D. E. Cartwright, K. Enke, J. A. Ewing, H. Gienapp, D. E. Hasselmann, P. Kruseman, A. Meerburg, P. Muller, D. J. Olbers, K. Richter, W. Sell and H. Walden, 1973: Measurements of wind–wave growth and swell decay during the Joint North Sea Wave Project (JONSWAP) *Dtsch. Hydrogr. Z.*, **A8**(Suppl.), No. 12, 95 pp.

——, 1974: On the spectral dissipation of ocean waves due to white-capping. *Bound.-Layer Meteor.*, **6,** 107–127.

Holthuijsen, L., 1981: The direction energy distribution of wind generated waves as inferred from stereophotographic observations of the sea surface. Rep. 81-2., Dept. Civ. Eng., Delft University of Technology, 193 pp.

——, 1983: Observations of the directional distribution of ocean-wave energy in fetch-limited conditions. *J. Phys. Oceanogr.*, **13,** 191–207.

Jackson, F. C., W. T. Walton and P. L. Baker, 1985a: Aircraft and satellite measurement of ocean wave directional spectra using scanning beam microwave radars. *J. Geophys. Res.*, **90,** 987–1004.

——, and C. Y. Peng, 1985b: A comparison of in situ and airborne radar observations of ocean wave directionality. *J. Geophys. Res.*, **90,** 1005–1018.

Kahma, K. K., 1981: A study of the growth of the wave spectrum with fetch. *J. Phys. Oceanogr.*, **11,** 1503–1515.

Kawai, S., K. Okuda and Y. Toba, 1977: Field data support of three seconds power law and $gu_*\omega^{-4}$ spectral form for growing wind waves. *J. Oceanogr. Soc. Japan,* **33,** 137–150.

Kitaigorodskii, S. A., 1983: On the theory of the equilibrium range in the spectrum of wind-generated gravity waves. *J. Phys. Oceanogr.*, **13,** 816–827.

——, V. P. Krasitskii and M. M. Zaslavskii, 1975: On Phillips' theory of equilibrium range in the spectra of wind-generated gravity waves. *J. Phys. Oceanogr.*, **5,** 410–420.

Komen, G. J., S. Hasselmann and K. Hasselmann, 1984: On the existence of a fully developed wind-sea spectrum. *J. Phys. Oceanogr.*, **14,** 1271–1285.

Kondo, J., Y. Fujinawa and G. Naito, 1973: High-frequency components of ocean waves and their relation to the aerodynamic roughness. *J. Phys. Oceanogr.*, **3,** 197–202.

Leykin, I. A., and A. D. Rozenberg, 1984: Sea tower measurements of wind wave spectra in the Caspian Sea. *J. Phys. Oceanogr.*, **14,** 168–176.

Liu, P. C., 1989: On the slope of the equilibrium range in the frequency spectrum of wind waves. *J. Geophys. Res.*, **94,** 5017–5023.

Longuet-Higgins, M. S., D. E. Cartwright and N. D. Smith, 1963: Observations of the directional spectrum of sea waves using the motions of a floating buoy. *Ocean Wave Spectra,* Prentice Hall, 111–136.

McLeish, W., and D. B. Ross, 1983: Imaging radar observations of direction properties of ocean waves. *J. Geophys. Res.*, **88,** 4407–4419.

——, and ——, 1985: Reply to comment by F. C. Jackson and C. Y. Peng. *J. Geophys. Res.*, **90,** 7371–7375.

Mitsuyasu, H., 1977: Measurement of the high frequency spectrum of ocean surface waves. *J. Phys. Oceanogr.*, **7,** 882–891.

——, F. Tasai, T. Shuhara, S. Mizuno, M. Ohkuso, T. Honda and K. Rikiishi, 1975: Observations of the directional spectrum of ocean waves using a cloverleaf buoy. *J. Phys. Oceanogr.*, **5,** 750–760.

Pierson, W. J., and L. Moskowitz, 1964: A proposed spectral form for fully developed wind seas based on the similarity theory of S. A. Kitaigorodskii. *J. Geophys. Res.*, **69,** 5181–5190.

Phillips, O. M., 1958: The equilibrium range in the spectrum of wind-generated waves. *J. Fluid Mech.*, **4,** 426–434.

——, 1977: *The Dynamics of the Upper Ocean,* 2nd ed. Cambridge University Press.

——, 1981: The dispersion of short wavelets in the presence of a dominant long wave. *J. Fluid Mech.*, **107,** 465–485.

——, 1985: Spectral and statistical properties of the equilibrium range in wind-generated gravity waves. *J. Fluid Mech.*, **156,** 505–531.

——, and M. L. Banner, 1974: Wave breaking in the presence of wind drift and swell. *J. Fluid Mech.*, **66,** 625–640.

Schule, J. J., L. S. Simpson and P. S. DeLeonibus, 1971: A study of fetch-limited wave spectra with an airborne laser. *J. Geophys. Res.*, **76,** 4160–4171.

Snyder, R. L., F. W. Dobson, J. A. Elliott and R. B. Long, 1981: Array measurements of atmospheric pressure fluctuations over surface gravity waves. *J. Fluid Mech.*, **102,** 1–59.

Stolte, S., 1984: Modulation of short waves by long wind waves and wind. PhD Dissertation, University of Hamburg, 199 pp.

Toba, Y., 1973: Local balance in the air–sea boundary processes. Part III: On the spectrum of wind waves. *J. Oceanogr. Soc. Japan,* **29,** 209–220.

Walsh, E. J., D. W. Hancock, D. E. Hines, R. N. Swift and J. F. Scott, 1985: Directional wave spectra measured with the surface contour radar. *J. Phys. Oceanogr.*, **15,** 566–592.

Webb, D. J., 1978: Nonlinear transfers between sea waves. *Deep-Sea Res.*, **25,** 279–298.

Wu, J., 1975: Wind-induced drift currents. *J. Fluid Mech.*, **68,** 49–70.

——, 1980: Wind-stress coefficients over the sea surface near neutral conditions—a revisit. *J. Phys. Oceanogr.*, **10,** 727–740.

Young, I. R., S. Hasselmann and K. Hasselmann, 1987: Computations of the response of a wave spectrum to a sudden change in wind direction. *J. Phys. Oceanogr.*, **17,** 1317–1338.